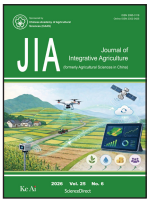
Journal of Integrative Agriculture 2026, 25(6): 2434–2448

Available online at ScienceDirect

Journal of Integrative Agriculture



RESEARCH ARTICLE

SlPIP1;7 enhances tomato acclimation to high VPD through optimizing stomatal morphology and regulating ROS

Yuhui Zhang[1, 2], Xuemei Yu[1, 2], Zhengda Zhang[3], Shuhui Zhang[1, 2], Jianming Li[1, 2#]

[1] *College of Horticulture, Northwest A&F University, Yangling 712100, China*
[2] *Key Laboratory of Protected Horticulture Engineering in Northwest, Ministry of Agriculture and Rural Affairs, Yangling 712100, China*
[3] *National Key Laboratory of Plant Molecular Genetics, CAS Center for Excellence in Molecular Plant Sciences (CEMPS), Institute of Plant Physiology and Ecology (SIPPE), Chinese Academy of Sciences (CAS), Shanghai 200032, China*

Highlights

- Identifies *SlPIP1;7* as a key gene for tomato adaptation to high vapor pressure deficit (VPD) stress.
- Overexpression enhances antioxidant activity, reducing ROS accumulation and atmospheric drought sensitivity.
- Optimizes stomatal morphology to improve water-use efficiency and CO_2 assimilation under high VPD.
- Reveals SlERF4 transcriptional regulation of *SlPIP1;7 via* Y1H and LUC validation.

Abstract

Vapor pressure deficit (VPD), defined as the difference between the actual water vapor pressure and the saturation vapor pressure in the air, is a core indicator of atmospheric aridity. High VPD induces intensified water loss *via* plant transpiration, thereby constraining water uptake and photosynthetic capacity. The dynamic functions and molecular regulatory mechanisms of plasma membrane intrinsic proteins (PIPs), key aquaporins mediating rapid transmembrane water transport, remain unclear during plant responses to high VPD stress. In this study, we elucidated the regulatory role of *SlPIP1;7* in regulating the multi-level adaptation strategy of tomato (*Solanum lycopersicum*) at the morphological, physiological, and molecular levels under high VPD conditions. The results indicate that, compared to wild-type (WT) plants, *SlPIP1;7* overexpressing (OE) plants exhibit superior growth performance under high VPD conditions. The overexpression of *SlPIP1;7* significantly enhances the reactive oxygen species (ROS) scavenging efficiency, effectively protecting plant cells from oxidative damage. This protective mechanism for maintaining ROS homeostasis is closely associated with stomatal function. The overexpression of *SlPIP1;7* can regulate stomatal morphology, size, and aperture dynamics, thereby promoting efficient utilization of water and carbon dioxide and enhancing the overall physiological regulatory capacity of plants under stress conditions. Additionally, we identified the ethylene response factor SlERF4 as an upstream regulatory factor in this adaptive network. Yeast one-hybrid (Y1H) and dual-luciferase (LUC) assays demonstrate that the transcription factor SlERF4 can bind to the *SlPIP1;7* promoter, enhancing its expression and functionality. This interaction further underscores the pivotal role of *SlPIP1;7* in combating high VPD stress. In summary, our study elucidates the crucial function of *SlPIP1;7* in plant response and acclimation to high VPD stress. These findings expand our understanding of the molecular mechanisms underlying plant acclimation to environmental stresses and provide a reference for future breeding strategies aimed at developing drought-resistant crops.

Keywords: tomato, vapor pressure deficit, plasma membrane aquaporins, leaf morphology

1. Introduction

Water is a critical element for plant growth and development. Extensive research has highlighted that water stress significantly impairs the normal growth of plants, with a predominant focus on soil moisture stress (Aroca *et al.* 2012; Rodriguez *et al.* 2016; Zhang *et al.* 2019). However, the increasing vapor pressure deficit (VPD) associated with global warming has recently emerged as a critical area of

Received 4 March 2025; Received in revised form 11 July 2025; Accepted 18 October 2025; Available online 16 April 2026
Yuhui Zhang, E-mail: zyh_0065@163.com; #Correspondence Jianming Li, E-mail: lijianming66@163.com

© 2026 CAAS. Publishing services by Elsevier B.V. on behalf of KeAi Communications Co. Ltd. This is an open access article under the CC BY-NC-ND license (http://creativecommons.org/licenses/by-nc-nd/4.0/). Peer review under responsibility of Editorial Board of *Journal of Integrative Agriculture*.
doi: 10.1016/j.jia.2026.04.020

concern (Li *et al.* 2023). High VPD significantly impacts the growth and physiological processes of tomato (*Solanum lycopersicum* L.) plants (Zhang *et al.* 2017; Buckley 2019; Yuan *et al.* 2019; Grossiord *et al.* 2020; Wang *et al.* 2020). Under high VPD conditions, the elevated transpiration rate accelerates soil moisture depletion, prompting plants to close their stomata as a strategy to minimize water loss (Zhang *et al.* 2018; Keenan *et al.* 2013; Mathias and Thomas 2021). However, this stomatal closure limits carbon dioxide uptake, thereby inhibiting photosynthesis and reducing the synthesis of photoassimilates (Ding J P *et al.* 2022). Additionally, high VPD can induce chlorophyll degradation, resulting in leaf yellowing and a decline in photosynthetic efficiency (Yu *et al.* 2023; Zhang D L *et al.* 2024). Prolonged exposure to high VPD conditions may also lead to the excessive accumulation of reactive oxygen species (ROS), which causes oxidative damage to cell membranes and other cellular components (Considine and Foyer 2021). Moreover, extensive studies have demonstrated that high VPD significantly reduces stomatal conductance, suppressing photosynthetic carbon assimilation and nutrient uptake, and ultimately leading to yield reductions. These effects have been widely validated not only in tomato but also in various other crops, such as gramineous crops (e.g., *Oryza sativa* and *Triticum aestivum*) (Medina *et al.* 2016; Fakhet *et al.* 2021; Koehler *et al.* 2023; Yu *et al.* 2024), oilseed crops (e.g., *Glycine max* and *Arachis hypogaea*) (Vadez *et al.* 2014), and fruit trees (e.g., *Prunus persica*, *Mangifera indica*, *Olea europaea*, *Citrus sinensis*, and *Eriobotrya japonica*) (Carella *et al.* 2023; Yamanaka *et al.* 2024). Furthermore, high VPD affects root development, nutrient uptake, and fruit quality (Grossiord *et al.* 2020), further aggravating its adverse effects on crop growth. Therefore, identifying and elucidating the adaptive mechanisms employed by plants under high VPD conditions, particularly with respect to water management strategies, is essential for improving crop stress tolerance.

Under conditions of stress, plant aquaporins (AQPs) play a crucial role. AQPs are a class of transmembrane proteins primarily responsible for the transport of water and small solutes (Bienert and Bienert 2017; Jing *et al.* 2023). Among the widely distributed AQPs in plants, the plasma membrane intrinsic proteins (PIPs) subfamily has been shown to play an important role in regulating water transport and responding to abiotic stresses, including drought, salinity, and extreme temperatures (Maurel *et al.* 2015; Zhou *et al.* 2019; Gautam and Pandey 2021; Kurowska 2021). PIP proteins, as integral membrane proteins, have their secondary structure closely linked to the formation and functionality of their channels. For example, the phosphorylation site at the C-terminus of AQP2 (e.g., Ser256) has been shown to modulate channel activity. In plants, the conformational changes in PIP proteins may regulate water uptake by dynamically adjusting the NPA motif (Hoffert *et al.* 2006; Olesen and Fenton 2021).

Studies have shown that increasing the expression levels of certain PIP proteins can enhance plant stress tolerance and improve their responses to adverse environmental conditions (Li *et al.* 2014). For instance, Ding L *et al.* (2022) found that the overexpression of *PIP2;5* in *Zea mays* L. influenced stomatal closure, reduced transpiration rates, and thereby improved water use efficiency and drought resistance. However, the effects of PIP proteins are not universally beneficial, as their functions may vary depending on specific isoforms. For example, in *Arabidopsis thaliana*, elevated expression of *PIP2;8* has been shown to inhibit stomatal closure, ultimately reducing the plant's drought tolerance (Liu *et al.* 2023). These findings highlight the complex roles of different PIP proteins in plant stress responses, underscoring the need for more detailed and in-depth studies to fully understand their functions.

Tomato is one of the most important vegetable crops worldwide, and its growth responses to adverse environmental conditions, particularly its acclimation to high VPD conditions, have become a research focus. Under high VPD, plants must respond rapidly to adjust the water balance between their internal and external environments to maintain physiological homeostasis. During this process, AQPs play a critical role in regulating stomatal opening and closure as well as efficient water transport, enabling plants to maintain a certain level of water use efficiency under high VPD conditions (Chaumont and Tyerman 2014; Groszmann *et al.* 2017). For instance, in *A. thaliana*, *AtPIP2;4* reduces water loss under high VPD by inhibiting excessive stomatal opening (Israel *et al.* 2021).

The PIP subfamily of aquaporins plays a particularly crucial role in plant responses to high VPD conditions. These proteins not only directly regulate transmembrane water transport but also mitigate osmotic imbalance caused by high VPD stress by accelerating water uptake and intracellular transport. Studies have shown that under high VPD conditions, the expression of many *SlTIP* and *SlPIP* genes in tomato is significantly upregulated, accompanied by increased stomatal conductance (Gs) and net assimilation rate. This process substantially optimizes water transport, further underscoring the pivotal role of PIP proteins in regulating plant responses to atmospheric drought (VPD) (Yu *et al.* 2022; Zhang Y H *et al.* 2024). Among the known response factors, the tomato gene *SlPIP1;7* has been identified as a key candidate for facilitating plant acclimation to adverse environmental conditions (Fan *et al.* 2021a, b). However, the specific mechanisms by which *SlPIP1;7* regulates tomato responses to high VPD stress remain largely unexplored. Elucidating the functional mechanisms of *SlPIP1;7* under high VPD environments is crucial for advancing our understanding of plant adaptive regulatory networks and enhancing crop stress resistance.

This study aims to systematically elucidate the regulatory mechanisms of the *SlPIP1;7* gene in tomatoes under high VPD stress, focusing on the following three key aspects: (1) regulation of ROS homeostasis: Evaluating whether *SlPIP1;7* mitigates oxidative damage by enhancing the activity of antioxidant enzymes; (2) optimization of stomatal morphology: Investigating the impact of *SlPIP1;7* on stomatal structure and gas exchange dynamics to establish an effective balance between carbon dioxide assimilation and water homeostasis; (3) transcriptional regulatory mechanisms: Identifying upstream regulators that modulate the expression of *SlPIP1;7* in response to stress conditions, such as ERF family transcription factors.

Through an in-depth examination of these mechanisms, our research will provide theoretical underpinning for two practical strategies: (1) employing molecular markers and other assisted selection techniques for the drought-resistant breeding of *SlPIP1;7* allelic variants; and (2) developing synthetic promoters that integrate SlERF4 binding sites with stress-inducible elements to finely regulate the expression levels of *SlPIP1;7* in crops.

2. Materials and methods

2.1. Experimental site and plant materials

In this experiment, the wild-type tomato variety 'Ailsa Craig' was used, along with *SlPIP1;7* overexpression (OE) tomato lines and *SlPIP1;7* RNA interference (RNAi) tomato lines generated through *Agrobacterium*-mediated transformation as experimental materials. These transgenic materials were generously provided by Professor Haijun Gong and Associate Professor Jia Guo from Northwest A&F University, China. Furthermore, previous studies have confirmed that the *SlPIP1;7*-OE lines play an important role under drought and salt stress, while the RNAi lines exhibit more than 70% specific gene silencing without off-target effects (Fan *et al.* 2021a, b). The cultivation of these plants followed methods outlined in previous research conducted by our team (Yu *et al.* 2022). The experimental setup began when the fifth true leaf of the tomato seedlings was fully expanded. The plants were placed in two identical climate-controlled chambers, each spanning 15 m^2, with the following environmental parameters set: a temperature of 25/18°C (day/night), a 14-hour photoperiod, and light intensity set at 800 μmol m^{-2} s^{-1}. The experiment included two different treatments based on VPD: low VPD and high VPD. In the low VPD treatment, VPD was 0.95 kPa (corresponding to an air humidity of 70±5%, the VPD environment suitable for tomato growth); in the high VPD treatment, the VPD was 2.22 kPa (corresponding to an air humidity control of 30±5%) (Li *et al.* 2019). The nutrition pots of each plant were covered with aluminum foil to prevent soil moisture dissipation. Following 12 days of treatment, assessments were conducted on gas exchange parameters, activities of enzymes in the antioxidant system, leaf anatomical structures, and staining experiments.

2.2. Measurement of gas exchange parameters

Gas exchange parameters were quantified utilizing the LI-6800 Portable Photosynthesis System (Li-Cor Inc., Lincoln, NE, USA), adhering to the methodology outlined by Zhang Y H *et al.* (2024). The CO_2 concentration in the leaf chamber was set to 400 μmol mol^{-1}, the temperature was maintained at 25°C, relative humidity of 70% (low VPD) and 30% (high VPD), and photosynthetic photon flux density (PPFD) was set to 1,000 μmol m^{-2} s^{-1}. These measurements were conducted on the third fully expanded leaf from five individual plants per treatment. Following the completion of these measurements, the same leaves were further analyzed to assess gene relative expression, stomatal morphology, and anatomical structure, providing a comprehensive view of the physiological and structural responses of the plants under different treatments.

2.3. Stomatal morphology

Stomatal morphology was observed under a light microscope (BX51+IX71, Olympus, Japan) following the protocol developed by Xu and Zhou (2008). The stomatal morphological characteristics were quantified using Image J software (National Institutes of Health, Bethesda, Maryland, USA). Key measurements included stomatal size, individual stomatal area, and stomatal density, with the latter being expressed as the number of stomata per unit leaf area. The calculation for individual stomatal area adheres to the formula: π/4×stomatal length×stomatal width, where π is approximated as 3.142 (Franks and Farquhar 2001).

2.4. Observation of leaf anatomical structure parameters and chloroplast ultrastructure

Leaf anatomical structure parameters were analyzed employing paraffin embedding techniques. Segments of leaf tissue, excluding major veins and measuring 4 mm^2, were excised and immediately fixed in FAA solution for 24 hours. Following dehydration, the sample was embedded in paraffin. Sections were stained for observation. Sections were cut and stained to obtain various parameters of leaf anatomy by observation under a light microscope (BX51+IX71, Olympus, Japan). Measurements were performed using ImageJ software, and 25 fields of view were examined for each treatment.

A 1 mm^3 piece of leaf was fixed in a 2.5% glutaraldehyde solution, which was prepared using 0.1 mol L^{-1} Phosphate Buffered Saline (PBS) at a pH of 7.2–7.4, for a duration exceeding 5 hours. Following this, the sample was rinsed with 0.1 mol L^{-1} PBS and subsequently fixed in 1% osmium tetroxide, also prepared with PBS, for 2–3 hours. This was succeeded by another rinsing phase with PBS. The sample then underwent dehydration through a graded ethanol series, ranging from 30 to 100%, and was embedded in resin. Sections approximately 70 nm thick were cut using an ultramicrotome (EM UC7, Leica, Germany) and stained with 2% uranyl acetate and lead citrate. The structure of chloroplasts within the sample was examined using a Tecnai G2 Spirit Bio transmission electron microscope (FEI, Czech Republic).

2.5. RNA extraction and qRT-PCR analysis

Total RNA from tomato was extracted following the procedure outlined by Zhang Z D *et al.* (2024). The RNA samples were then subjected to qRT-PCR analysis using the methodology established by Zhang Z D *et al.* (2022). Using the *Actin-7* gene as an internal reference gene. The relative gene expression was calculated according to the method of Livak and Schmittgen (2001). Each experimental condition was replicated three times biologically, and the sequences of gene-specific primers are detailed in Appendix A.

2.6. Determination of relevant physiological indices and histochemical staining

The activities of antioxidant system enzymes in our study were assessed using kits from Solarbio (Beijing, China). Specifically, the measurements included the contents of hydrogen peroxide (H_2O_2, BC3590), superoxide anion (O_2^{-}·,

BC1290), and malondialdehyde (MDA, BC0020), as well as the activities of catalase (CAT, BC0200), superoxide dismutase (SOD, BC0170), peroxidase (POD, BC0090) and ascorbate peroxidase (APX, BC0220) were determined according to the methods provided in the kits.

Histochemical staining techniques were employed to detect the accumulation of $O_2^{-}\cdot$ and H_2O_2 in tomato seedling leaves. Both staining procedures were performed following the methodologies outlined by Huang *et al.* (2013). Additionally, the relative electrical conductivity (REC) in tomato leaves was measured in accord with the protocol described by Zhou and Leul (1998). To evaluate the maximum quantum yield of PSII photochemistry (F_v/F_m), an Open FluorCam FC 800-O (PSI, Brno, Czech Republic) was utilized, following protocols from Pérez-Bueno *et al.* (2015).

2.7. Staining of ROS in stomata

The detection of ROS in guard cells was conducted using the fluorescent probe H_2DCF-DA (2′,7′-dichlorofluorescein diacetate), following the established protocol by Chater *et al.* (2015). The procedure involved treating the epidermal layers of tomato leaves with a 50 μmol L^{-1} H_2DCF-DA in a buffer solution. This was followed by a dark incubation period of 10 min. Post-incubation, the sections were washed with fresh identical buffer solution for an additional 10 min to eliminate any unbound probe. The fluorescence emitted was subsequently captured and imaged using a Leica TCS-SP8 laser scanning confocal microscope (Leica Microsystems GmbH, Heidelberg, Germany), with an excitation wavelength of 488 nm.

2.8. Subcellular localization and bioinformatics analysis of SlPIP1;7 protein

Firstly, the coding region of *SlPIP1;7* lacking the TAA stop codon was cloned and subsequently inserted into the pCAMBIA2300 vector. The resultant fusion vectors were independently transformed into tobacco leaf tissues using the transformation protocol described by Zhang Z D *et al.* (2023). Following this transformation, the tobacco plants were kept in the dark for 48 hours, after which they were exposed to normal light conditions for 24 hours prior to sample collection for analysis. The transgenic tobacco leaf samples were examined and imaged using a Leica TCS-SP8 laser scanning confocal microscope. The transformation process for control organelle marker vectors followed the same protocol, employing myr-mCherry as the cell membrane marker as detailed by Du *et al.* (2021). Primers utilized in the construction of the vector are detailed in Appendix A, and the websites employed for bioinformatics analysis are enumerated in Appendix B.

2.9. Dual luciferase (LUC) assay

The LUC assay was conducted according to the method described by Zhang Y H *et al.* (2024) with recombinant vectors containing the target gene *SlERF4* and *SlPIP1;7* promoter transiently co-expressed in tobacco leaves. Leaf discs were taken and LUC activity was measured using a Dual-Luciferase Reporter Assay Kit (Yeasen Biotechnology, Shanghai, China), and the relative LUC activity was quantified using a 96-well microplate reader. The primers employed in the construction of vectors are detailed in Appendix A.

2.10. Yeast one-hybrid (Y1H) assay

This study utilized the Y1H system. The coding sequence (CDS) of *SlERF4* and promoter sequence of *SlPIP1;7* were cloned into the pGADT7 and pAbAi vectors, respectively. The recombinant vectors were co-transformed into competent yeast strains. The yeast transformations were performed using the Yeast Transformation Kit (Coolaber, Beijing, China), and the yeast strain used was the Y1H strain. Protein-DNA interactions were examined on SD–Ura–Leu medium supplemented with aureobasidin A (AbA). The primers employed in the construction of vectors are detailed in Appendix A.

2.11. Data analysis

The one-way analysis of variance (ANOVA) was conducted to analyze the data utilizing SPSS 20.0 software (IBM Corp., Armonk, NY, USA). Treatment differences were assessed with Tukey's test, considering differences significant at a *P*-value less than 0.05.

3. Results

3.1. Subcellular localization and bioinformatics analysis of SlPIP1;7

Transient overexpression of GFP-tagged *SlPIP1;7* in tobacco showed its signal overlapped with the membrane localization marker (myr-mCherry), confirming that SlPIP1;7 is located on the plasma membrane (Fig. 1-C). *Cis*-acting element analysis revealed a multitude of core elements (CAAT-box, TATA-box) as well as light-responsive elements, and also elements responding to ethylene response element (ERE) present in its promoter region (Appendix C). This finding indicates that the expression of the *SlPIP1;7* gene may be subject to complex regulatory mechanisms involving light exposure and specific transcription factors. Further, secondary structure analysis identified that the SlPIP1;7 protein is composed of α-helices and random coils (Appendix D-a). Advancing this analysis, a tertiary structure model for the SlPIP1;7 protein was generated (Appendix D-b). Assessment through Ramachandran plot showed that while there was one amino acid residue located in the disallowed region, the distribution of the remaining residues was favorable, with 78.3% in the most favored region, 18.7% in additional allowed regions, and 2.5% in generously allowed regions (Appendix D-c). This evaluation indicates that the constructed model of the tertiary structure of the SlPIP1;7 protein has an overall high degree of reliability.

3.2. Overexpression of *SlPIP1;7* enhances tomato tolerance to high VPD

After 12 days of high VPD treatment, a significant superiority in growth was observed in *SlPIP1;7* overexpressing tomato plants relative to RNAi-interfered plants. However, their growth size was not significantly different from that of the wild-type plants. Under low VPD conditions, the phenotypic differences between the overexpression and

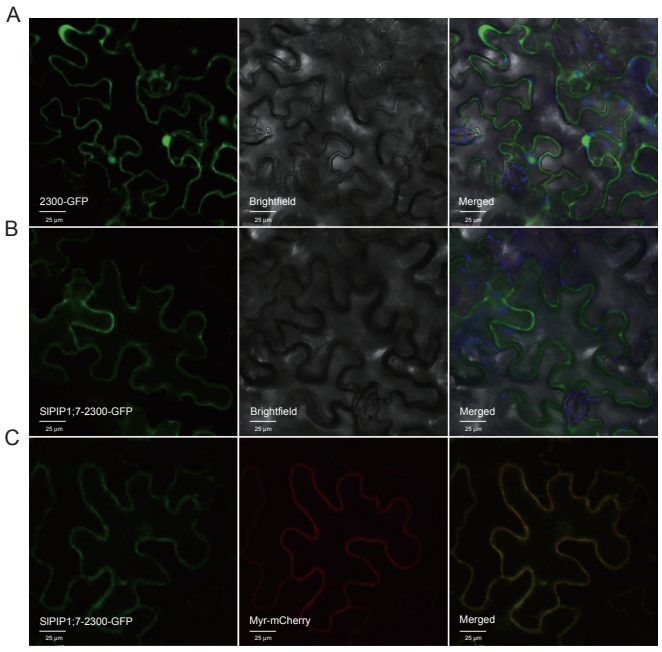


Fig. 1 Localization of SlPIP1;7 on the plasma membrane. A, tobacco leaves were transformed with the empty vector pCAMBIA2300-GFP. B, tobacco leaves were transformed with the fusion vector pCAMBIA2000-*SlPIP1;7*. C, tobacco leaves were co-transfected with the fusion vector pCAMBIA2000-*SlPIP1;7* and a cytoplasmic membrane marker (myr-mCherry). Scale bar=25 μm.

RNAi lines were not significant (Fig. 2-A). Analysis of MDA concentration and REC under high VPD conditions indicated that the *SlPIP1;7* overexpressing lines had significantly lower MDA concentration (Fig. 2-B) and REC (Fig. 2-B) compared to WT, with an observed increase in F_v/F_m (Fig. 2-C; Appendix E). Conversely, the *SlPIP1;7* RNAi lines showed a notable rise in MDA concentration and REC, while exhibiting a decrease in F_v/F_m. Under low VPD conditions, the RNAi lines displayed significantly higher MDA concentration and REC compared to WT, marked by a dip in F_v/F_m. However, even though REC were significantly elevated in the overexpressing lines in comparison to WT under the same conditions, the MDA concentration and F_v/F_m were not significantly different from those of WT.

3.3. Anatomical structure and chloroplast ultrastructure of *SlPIP1;7* transgenic plant leaves

Under high VPD conditions, compared to the WT lines, the T_{leaf} and $T_{palisade}$ in the overexpressing line *SlPIP1;7*-OE#32 significantly increased, while the T_{sponge} and the $T_{p/s}$ significantly decreased. In the *SlPIP1;7*-OE#15 overexpressing line, T_{leaf}, T_{sponge}, and $T_{palisade}$ significantly decreased, while $T_{p/s}$ showed no significant change. Meanwhile, in the RNAi lines, T_{leaf}, T_{sponge}, and $T_{palisade}$ significantly decreased compared to the WT lines (Table 1).

Under low VPD levels, compared to the WT lines, $T_{palisade}$ significantly decreased in the *SlPIP1;7* overexpressing lines,

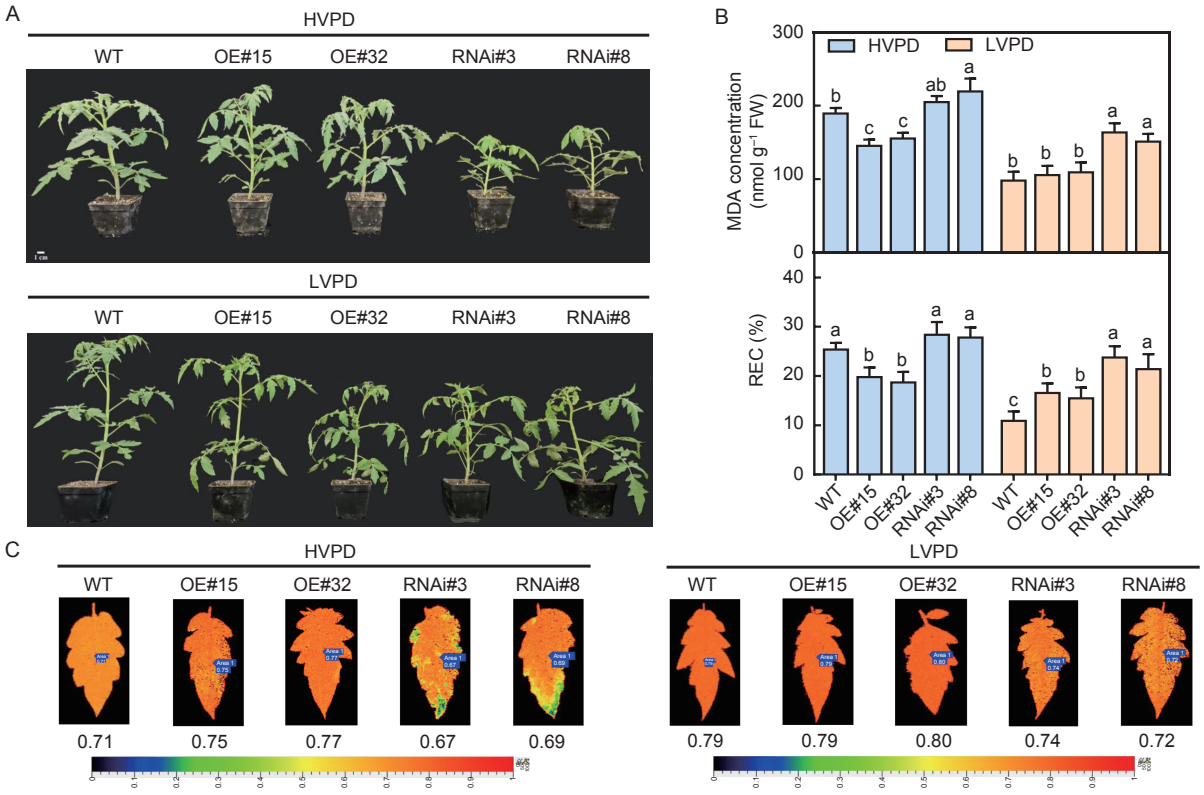


Fig. 2 *SlPIP1;7* can improve the adaptability of tomato plants under high vapor pressure deficit (VPD). A, phenotypes of *SlPIP1;7* overexpression and RNAi interference plants versus WT tomato lines under high and low VPD treatments (HVPD and LVPD, respectively). B and C, MDA concentration and REC values (B) and F_v/F_m (C) in leaves of *SlPIP1;7* overexpression and RNAi interference plants and WT tomato lines. Distinct letters attached to the data indicate significant differences among treatments (P<0.05).

while T_{leaf} and $T_{p/s}$ showed no significant differences; in the *SlPIP1;7* RNAi lines, T_{leaf}, T_{sponge}, and $T_{palisade}$ significantly decreased, except for $T_{p/s}$, which showed no significant difference. Additionally, regardless of the VPD levels, T_{leaf}, T_{sponge}, and $T_{palisade}$ in the *SlPIP1;7* overexpressing lines were significantly higher than in the RNAi lines (Table 1).

Subsequent observations of chloroplast ultrastructure revealed that, compared to low VPD conditions, the accumulation of starch in leaves under high VPD conditions increased (Fig. 3-K–T). Compared to the WT lines, the accumulation of starch was markedly reduced in the lines overexpressing *SlPIP1;7*, whereas it increased in the RNAi lines.

3.4. Gas exchange parameters in *SlPIP1;7* transgenic plants

Under high VPD conditions, compared to the WT lines, the *SlPIP1;7* overexpressing lines (*SlPIP1;7*-OE#15 and *SlPIP1;7*-OE#32) exhibited significant physiological advantages. Specifically, the net assimilation rate (A) increased by 21.97 and 15.49%, the intercellular CO_2 concentration (C_i) significantly increased by 12.06 and 18.18%, the stomatal conductance (g_{sw}) increased by 29.79 and 38.3%, and the instantaneous water use efficiency ($WUE_{instant}$) significantly improved by 49.88 and 57.65%, respectively. Meanwhile, the transpiration rate (E) significantly decreased by 19.28 and 26.19%, and the stomatal limit value (L_s) also significantly decreased by 18.42 and 28.95%.

In contrast, compared to the WT lines, in the *SlPIP1;7*-RNAi#3 and *SlPIP1;7*-RNAi#8 lines, the A decreased by 12.11 and 22.82%, E increased by 21.43 and 15.48%, among which $WUE_{instant}$ in *SlPIP1;7*-RNAi#8 line significantly decreased by 32.94%. Among these indices, in the OE lines, A, C_i, g_{sw}, and $WUE_{instant}$ were higher, while E and L_s were lower than in the RNAi lines (Fig. 4-A–F).

The results under low VPD were similar to those under

Table 1 Characteristic parameters of leaf blade anatomy[1)]

Treatment[2)]	T_{leaf} (μm)	T_{sponge} (μm)	$T_{palisade}$ (μm)	$T_{p/s}$
HVPD				
WT	143.67±11.41 b	52.84±6.70 a	65.84±9.25 b	0.82±0.17 b
OE#15	132.70±14.26 c	44.90±5.62 b	59.15±11.21 c	0.78±0.15 b
OE#32	157.78±14.34 a	46.94±7.18 b	74.93±12.18 a	0.64±0.14 c
RNAi#3	114.22±11.87 d	35.70±5.33 d	48.46±8.84 d	0.76±0.17 b
RNAi#8	116.29±12.01 d	39.92±6.18 c	44.94±9.33 d	0.93±0.26 a
LVPD				
WT	138.75±11.27 a	48.20±6.50 a	66.34±10.05 a	0.75±0.17 a
OE#15	134.05±10.49 a	47.55±6.69 ab	60.15±6.67 b	0.80±0.13 a
OE#32	139.20±23.25 a	44.94±8.52 b	60.86±14.17 b	0.77±0.18 a
RNAi#3	106.81±9.71 b	36.03±4.47 c	47.01±6.91 c	0.78±0.15 a
RNAi#8	102.35±9.27 b	33.27±4.79 c	42.81±6.62 c	0.79±0.13 a

[1)] T_{leaf}, leaf thickness; T_{sponge}, spongy tissue thickness; $T_{palisade}$, palisade tissue thickness; $T_{p/s}$, palisade tissue thickness-to-spongy tissue thickness ratio.
[2)] HVPD and LVPD, high and low vapor pressure deficit (VPD), respectively.
Data are means±SE (n=25 images). Distinct letters attached to the data indicate significant differences among treatments (P<0.05).

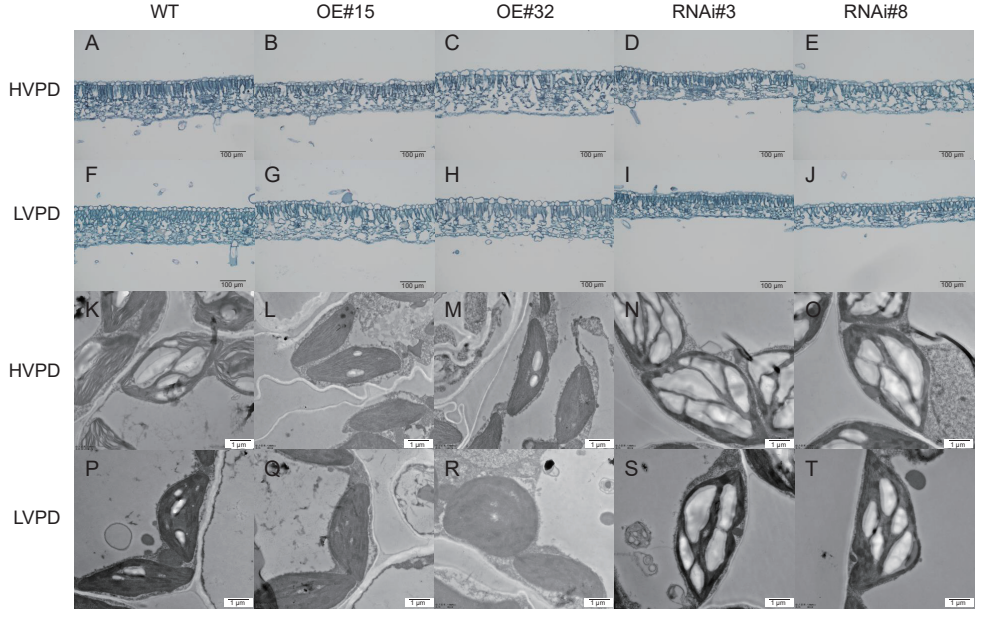


Fig. 3 Leaf anatomical structure (A–J) and chloroplast anatomical structure (K–T) after vapor pressure deficit (VPD) treatment. HVPD and LVPD, high and low VPD, respectively.

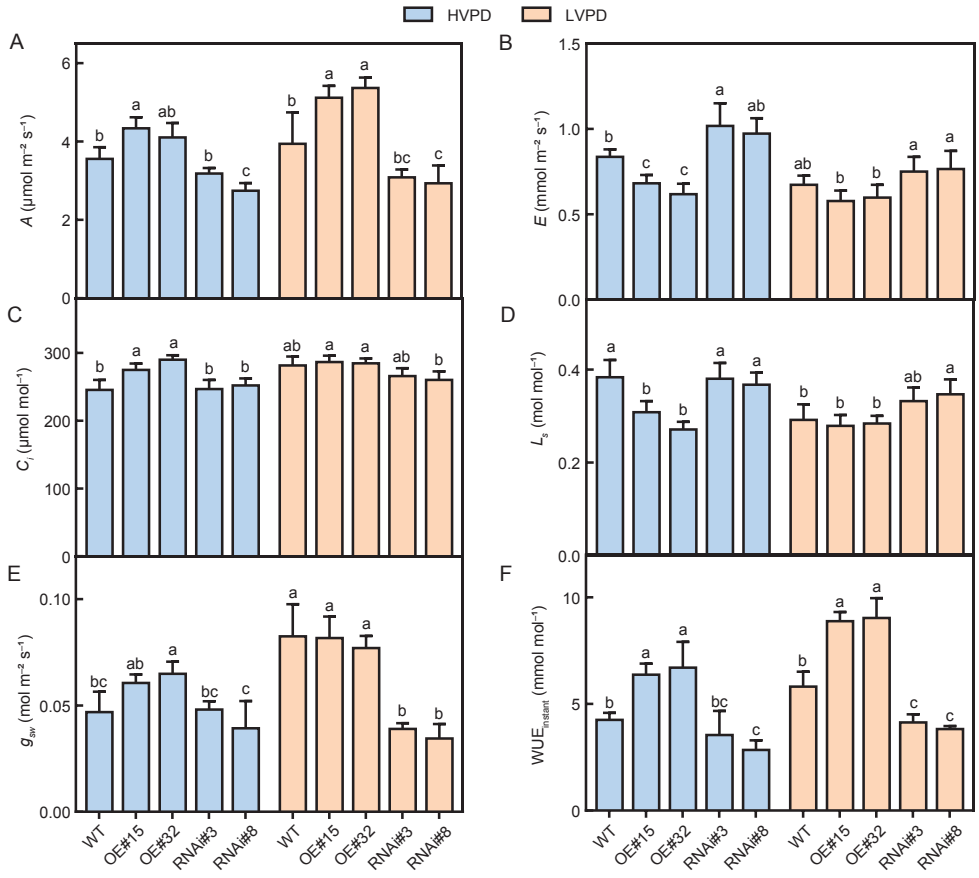


Fig. 4 Gas exchange parameters under vapor pressure deficit (VPD) treatment. A, net assimilation rate (*A*). B, transpiration rate (*E*). C, intercellular CO_2 concentration (C_i). D, stomatal limit value (L_s). E, stomatal conductance (g_{sw}). F, instantaneous water use efficiency ($WUE_{instant}$). HVPD and LVPD, high and low VPD, respectively. Distinct letters attached to the data indicate significant differences among treatments (P<0.05).

high VPD, with *A* and $WUE_{instant}$ in the OE lines being significantly higher than those in the WT lines, while no significant differences were observed in other parameters. Meanwhile, in the RNAi lines, *A*, g_{sw}, and $WUE_{instant}$ were all lower than in the WT lines. Comparisons between the OE and RNAi lines showed consistency under both high and low VPD conditions.

3.5. Stomatal morphological parameters in *SlPIP1;7* transgenic plant leaves

Under high VPD conditions, compared to the WT lines, the stomatal length, stomatal width, and single stomata area in the OE lines were significantly increased, with no significant difference in stomatal density (Fig. 5-A–D). Moreover, compared to WT lines, the stomatal density in the RNAi lines significantly decreased, while there was no significant difference in stomatal length and single stomata area. Additionally, all stomatal morphological parameters in the OE lines were significantly higher than those in the RNAi lines. The situation under low VPD treatment was similar to that under high VPD.

3.6. The impact of *SlPIP1;7* on the ROS scavenging ability in tomato plants

High VPD treatment led to an increase in the concentration of H_2O_2 and $O_2^{\cdot-}$ in tomato leaves. However, under high VPD, the OE lines exhibited lower ROS concentration and accumulation. Compared to the WT lines, the H_2O_2 concentration in *SlPIP1;7*-OE#15 and *SlPIP1;7*-OE#32 lines decreased by 18.45 and 6.88%, respectively, while the $O_2^{\cdot-}$ concentration decreased by 46.55 and 34.48%. At the same time, compared to WT and OE lines, the RNAi lines showed an increase in both H_2O_2 and $O_2^{\cdot-}$ concentration.

Under low VPD conditions, compared to the WT lines, the concentration of H_2O_2 and $O_2^{\cdot-}$ in the OE lines showed no significant difference, while in the RNAi lines, the concentration of $O_2^{\cdot-}$ increased by 1.76 and 1.47 times compared to the WT lines, with no significant difference in the H_2O_2 concentration (Fig. 6-A and B).

The results of histochemical staining of tomato tissues further confirmed these observations. After high VPD treatment, the accumulation of H_2O_2 and $O_2^{\cdot-}$ increased in the leaves of both WT and RNAi tomato lines; while in the leaves of the OE lines, the accumulation of H_2O_2 and $O_2^{\cdot-}$ was reduced (Fig. 6-C).

Additionally, we measured the activity of antioxidant enzymes within the plants and found that under high VPD conditions, compared to the WT lines, the activities of SOD, POD, CAT, and APX were all increased in the OE lines. In the RNAi lines, the activities of these ROS-scavenging

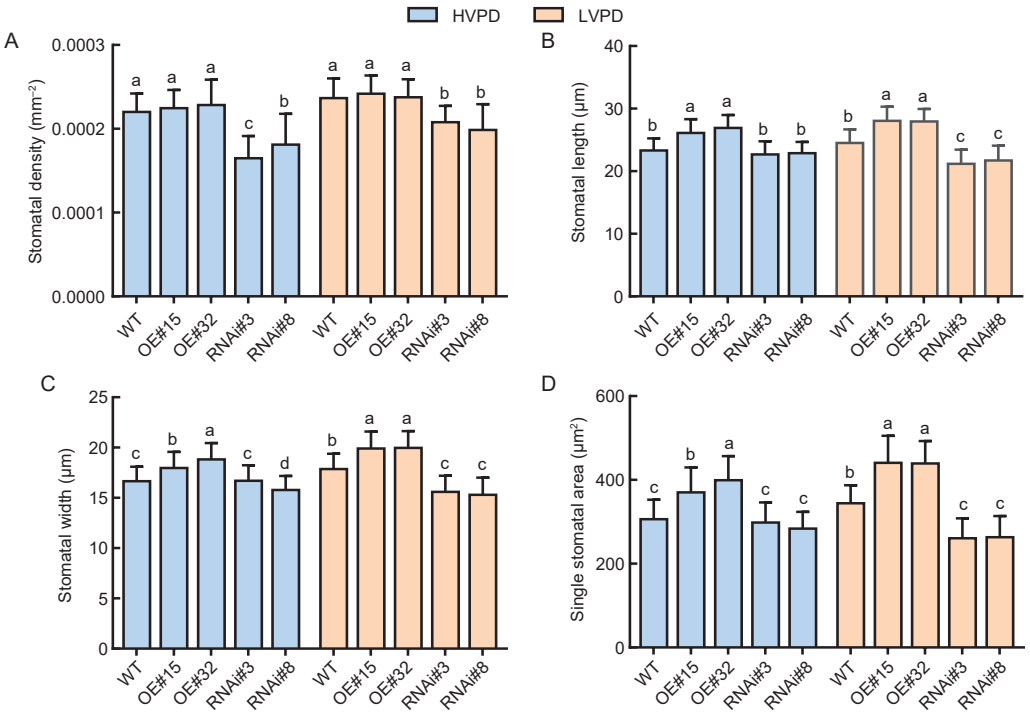


Fig. 5 Stomatal morphology parameters after vapor pressure deficit (VPD) treatment. A, stomatal density. B, stomatal length. C, stomatal width. D, single stomatal area. HVPD and LVPD, high and low VPD, respectively. Distinct letters attached to the data indicate significant differences among treatments (P<0.05).

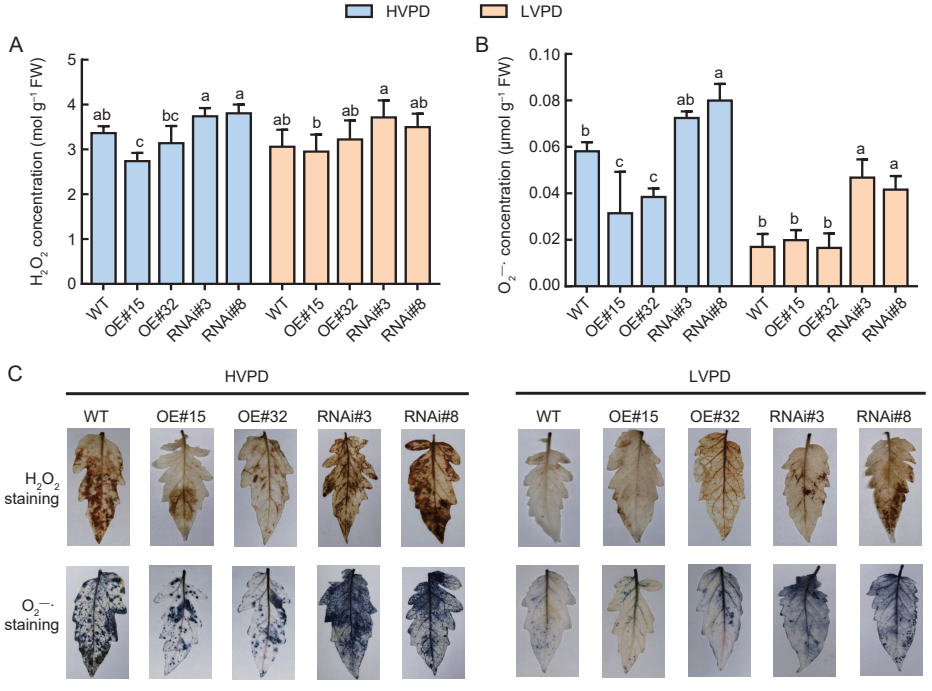


Fig. 6 *SlPIP1;7* alleviates reactive oxygen species (ROS) accumulation in tomato leaves under high vapor pressure deficit (VPD). A, H_2O_2 concentration in tomato seedlings leaves. B, $O_2^{\cdot-}$ concentration in tomato seedlings leaves. C, accumulation of H_2O_2 and $O_2^{\cdot-}$ in leaves of WT and transgenic tomato lines under different treatments. Tomato leaves were stained with DAB for H_2O_2 and NBT for $O_2^{\cdot-}$. HVPD and LVPD, high and low VPD, respectively. Distinct letters attached to the data indicate significant differences among treatments (P<0.05).

enzymes were decreased (Fig. 7-A–D).

The results of stomatal fluorescence staining indicated that high VPD treatment increased the accumulation of ROS within the stomata (Fig. 8), which was visually represented

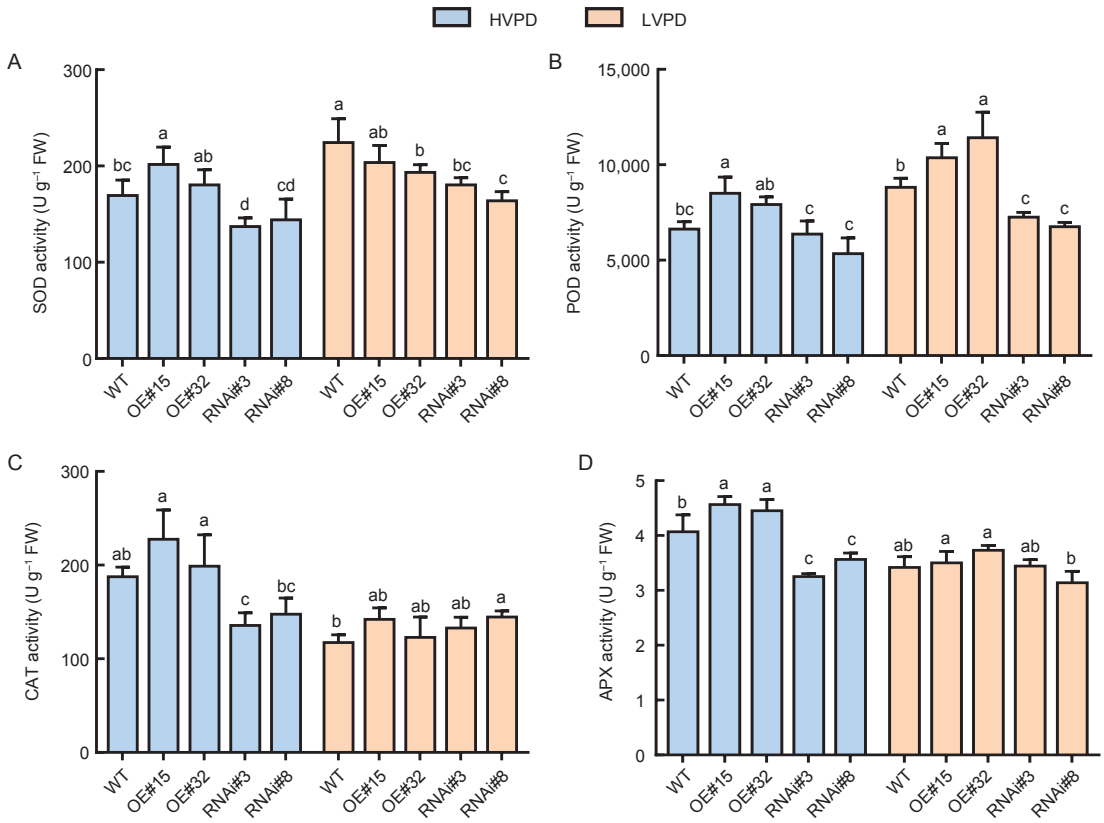


Fig. 7 *SlPIP1;7* enhances antioxidant enzyme activities in tomato leaves under high vapor pressure deficit (VPD). A–D, superoxide dismutase (SOD), peroxidase (POD), catalase (CAT), and ascorbate peroxidase (APX) activities in leaves of tomato seedlings. HVPD and LVPD, high and low VPD, respectively. Distinct letters attached to the data indicate significant differences among treatments (P<0.05).

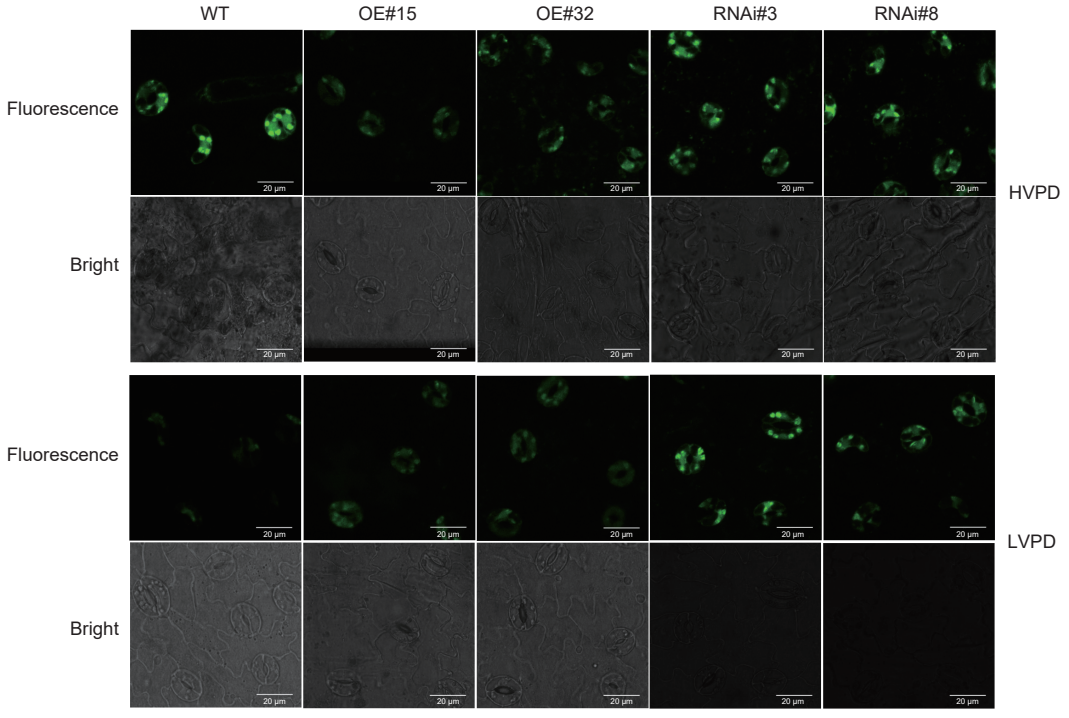


Fig. 8 Accumulation of stomatal reactive oxygen species (ROS) in tomato leaves. Under the fluorescence field, the green color represents the accumulation of ROS. HVPD and LVPD, high and low vapor pressure deficit, respectively.

by a stronger intensity of green fluorescence. In contrast, the accumulation of ROS within the stomata of tomato leaves in the OE lines was less, with a relatively weaker intensity of green fluorescence.

3.7. The transcription factor SlERF4 binds to the promoter of *SlPIP1;7* and activates its expression

Through the analysis of the *cis*-acting elements in the promoter of *SlPIP1;7*, we identified potential ethylene-responsive factor (ERF) binding sites (Appendix C). Preliminary yeast hybrid library screening suggested that the expression of *SlPIP1;7* might be regulated by the transcription factor SlERF4. To confirm the results of yeast screening, we employed Y1H system for validation. Initially, we constructed a vector pAbAi-P3 containing the *SlPIP1;7* promoter fragment (P3) (as shown in Fig. 9-A) and transformed it into Y1H yeast competent cells. The results indicated that self-activation of pAbAi-P3 was inhibited when the concentration of AbA was at 600 ng mL^{-1}. The study showed that pGADT7-*SlERF4*+pAbAi-P3 could grow normally on the selective medium containing 600 ng mL^{-1} of AbA, whereas the control group pGADT7+pAbAi-P3 could not grow, suggesting that SlERF4 is capable of binding to the promoter of *SlPIP1;7* (Fig. 9-B). Further LUC assays also validated the regulatory mechanism of SlERF4 on *SlPIP1;7*. We chose the *SlPIP1;7* promoter fragment (P3) to construct the reporter gene vector pGreen0800-P3 and conducted co-transformation experiments. The results showed that the LUC/REN ratio in the SK-*SlERF4* effector and reporter co-transformed was significantly higher than that in the control group (Fig. 9-C), further indicating that SlERF4 can bind to the *SlPIP1;7* promoter in tobacco. Additionally, high VPD significantly increased the expression of *SlERF4* in tomato seedling leaves, consistent with the expression pattern of *SlPIP1;7*, supporting the notion that SlERF4 might be directly involved in the response of tomato to high VPD through regulating *SlPIP1;7* (Fig. 9-D).

4. Discussion

This study comprehensively analyzed the effects of *SlPIP1;7* on tomato plants under various VPD conditions, defining the significant role of this gene in enhancing plant physiological adaptability and stress tolerance. The comparisons among *SlPIP1;7* OE lines, *SlPIP1;7* RNAi lines, and WT lines revealed the crucial role of this aquaporin in plant stress resistance. Under low VPD conditions, *SlPIP1;7* had no significant impact on plant water status and photosynthesis. Under excessive VPD conditions, *SlPIP1;7* was involved in regulating oxidative stress responses and played a key role in regulating stomatal conductance, water transpiration, and gas exchange. The mechanisms by which *SlPIP1;7* alleviates water stress under excessively high VPD conditions may involve three aspects: (1) Under high VPD conditions, *SlPIP1;7* activated antioxidant defense systems, reducing ROS concentration and thus mitigating the effects of air dryness. (2) *SlPIP1;7* optimized leaf structure, regulated water balance and gas exchange, to enhance photosynthesis and CO_2 absorption. (3) The transcription factor ERF4 participated in the transcriptional activation of *SlPIP1;7*.

4.1. *SlPIP1;7* is involved in the regulation of oxidative stress response

High VPD conditions exacerbated the accumulation of ROS within tomato leaves, further intensifying oxidative stress responses (Fig. 6). Despite the known influence of PIP aquaporins on the homeostasis of ROS (Bienert *et al.* 2007; Li G S *et al.* 2024), *SlPIP1;7* exhibits distinct regulatory characteristics, suggesting that it may enhance plant stress resistance through multiple pathways and levels. Research

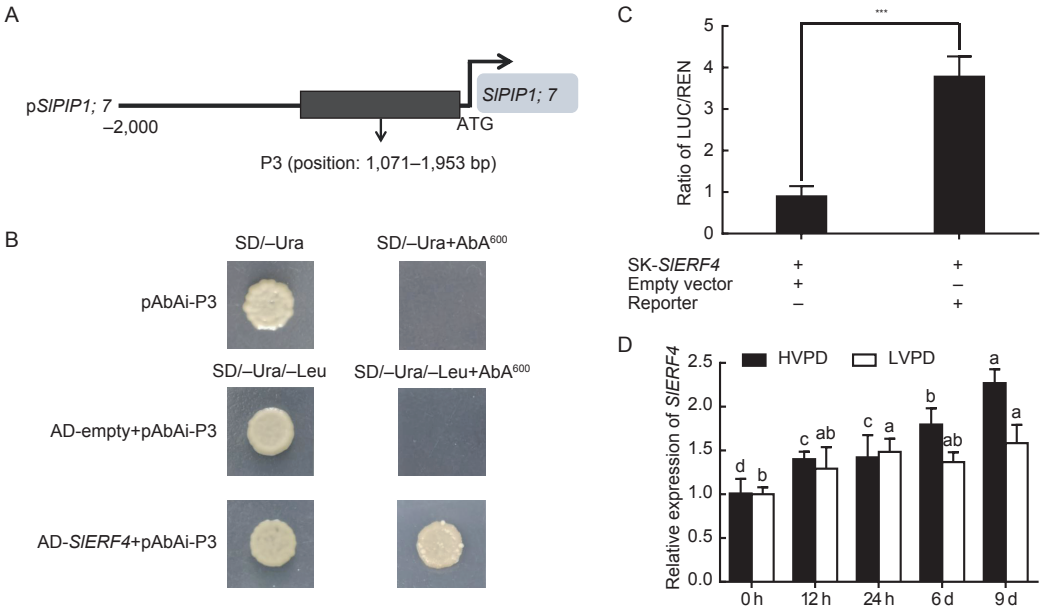


Fig. 9 The TF SlERF4 binds to the *SlPIP1;7* promoter and activates its expression. A, schematic representation of the *SlPIP1;7* promoter, with the black rectangle indicating the position of the partial promoter fragment (P3). B, Y1H assay showing that *SlERF4* binds to the promoter region of the *SlPIP1;7* promoter. C, various combinations of vectors were performed in the LUC assay (***, $P<0.05$). D, *SlERF4* expression in tomato leaves ($P<0.05$). HVPD and LVPD, high and low vapor pressure deficit, respectively.

has shown that certain plant kinases, such as Heat Shock Protein 90 (HSP90), Mitogen-Activated Protein Kinase (MAPK), and calcium-dependent protein kinases (CPKs), can interact with aquaporins to modulate their functionality by phosphorylation in response to environmental stress (Kozeko 2019; Majeed *et al.* 2023; Ravi *et al.* 2023). For instance, the study by Zhu *et al.* (2025) indicates that CPK28 activates H_2O_2 transport by interacting with and phosphorylating *PIP2;7* in Arabidopsis, thereby regulating the plant immune response. In the case of *SlPIP1;7*, specific kinases may enhance its transport capacity for H_2O_2 by phosphorylating active sites, leading to conformational changes. This mechanism can effectively assist plants in coping with ROS accumulation. Furthermore, in this study, overexpression of *SlPIP1;7* significantly increased the activity of SOD, POD, CAT, and APX (Fig. 7-A–D). This synergistic regulatory mechanism among multiple enzymes provides enhanced antioxidant capacity for plants to address multiple environmental stresses.

Unlike most PIP2 subfamily members that transport H_2O_2 through passive diffusion (Hooijmaijers *et al.* 2012; Zhang M *et al.* 2022; Yu F F *et al.* 2023; Li X T *et al.* 2024), *SlPIP1;7* may actively participate in the transport of H_2O_2 due to its unique channel structure. Secondary structure analysis indicates that the PIP1;7 protein primarily consists of α-helices and random coils, with its transmembrane regions enriched with hydrophobic residues (such as Val and Leu). These hydrophobic residues not only stabilize the protein's membrane integration *via* α-helices but also provide structural support for substance exchange and cellular interactions. Additionally, the PIP1;7 protein adopts a characteristic tetrameric form, with structural symmetry maintained by hydrogen bonds and hydrophobic interactions, which are essential for its functional stability. This structural arrangement enhances the mechanical strength and functional stability of the channel protein, allowing it to perform its functions efficiently within the cellular environment. Existing studies have shown that PIP proteins can be classified into multiple subfamilies (such as PIP1 and PIP2), with their functional differences being partially attributed to the fine-tuning of secondary structures. For example, the β-sheet structures in PIP2 subfamily members may enhance their ability to respond to environmental stress, while the α-helical structures in the PIP1 subfamily support the maintenance of cellular homeostasis (Törnroth-Horsefield *et al.* 2006; Tchakal-Mesbahi *et al.* 2024). These structural differences provide a critical basis for the functional specialization among diverse subfamilies.

Ramachandran plot analysis identified a conserved histidine residue (H132) in its second transmembrane helix, which may facilitate the transport of H_2O_2 through proton coupling (Appendix D-c). This hypothesis provides a new perspective for exploring and elucidating the active role of PIP aquaporins in ROS management. Moreover, the transport of H_2O_2 may also influence the activity of other antioxidant enzymes, such as SOD, CAT, and POD, through feedback mechanisms, thus forming a dynamic regulatory network to maintain the cellular redox balance (Veal *et al.* 2007; Hossain *et al.* 2015). Research indicates that H_2O_2 acts as a signaling molecule capable of activating genes associated with the antioxidant response, further enhancing the plant's adaptability to stress. For instance, H_2O_2 can induce the expression of APX, thereby facilitating the positive regulation of ROS levels (Smirnoff and Arnaud 2019). This association suggests that *SlPIP1;7* not only plays a role in the transport of ROS but may also enhance the overall stress resistance of plants by regulating H_2O_2 levels and influencing the expression of downstream genes.

The results of the ROS staining assay in stomata further support this finding (Fig. 8). *SlPIP1;7* helps maintain ion and metabolic balance within plant cells by enhancing antioxidant enzyme activity, thereby protecting cellular structures from oxidative damage. The downregulation of the *SlPIP1;7* gene can lead to decreased water stress tolerance, further confirming its critical role in the adaptation of plants to high VPD conditions. Additionally, as an aquaporin, *SlPIP1;7* aids in reducing ROS production induced by water stress by optimizing water transport and distribution (Maurel and Plassard 2011). Similar findings have indicated that overexpression of *OsPIP1* in rice (*Oryza sativa*) can enhance cold tolerance (Matsumoto *et al.* 2009). *OsPIP2;2* facilitates water transport and H_2O_2 transport to improve drought and alkalinity tolerance (Bai *et al.* 2021; Zhang Y *et al.* 2023). Furthermore, tobacco plants with reduced *PIP1* expression have shown lower water stress tolerance (Kaldenhoff and Fischer 2006; Sun *et al.* 2017). In summary, our findings confirm that *SlPIP1;7* plays an important role not only in the regulation of ROS levels but also in actively influencing stomatal regulation and the overall stress resistance of plants.

4.2. *SlPIP1;7* acclimates to high VPD through regulation of gas exchange and optimization of leaf structure

In this study, significant changes were observed in the leaf structure of *SlPIP1;7* overexpression plants, including increased leaf thickness and decreased thickness of both spongy and palisade tissues. These characteristics reflect the plant's adaptive strategies under high VPD conditions. Specifically, the increase in palisade tissue thickness serves to extend the path of photon transport within the photosynthetic cells, thereby enhancing light capture capacity (Tamang *et al.* 2023). This is directly correlated with the significant increase in *A* observed (Fig. 4-A). Simultaneously, the compressed spongy tissue effectively reduces the internal air space by decreasing intercellular air gaps, subsequently minimizing the effective diffusion pathway for water vapor (Buckley 2019) and significantly suppressing the transpiration rate (Fig. 4-B). Furthermore, the increase in leaf thickness contributes to the reduction of water evaporation, acting as a mechanism for adaptation to drought stress (John *et al.* 2017). This process, in conjunction with the adjustments in stomatal morphology (Fig. 5-B–D), establishes a multi-tiered network for moisture regulation.

It is well known that the g_{sw} of plant is determined by stomatal density and size, both of which are intricately related to the growth environment (Yong *et al.* 1997; Liu *et al.* 2019). Under high VPD conditions, plants generally exhibit reduced

stomatal size and density. This modification reduces carbon assimilation, which consequently lowers the efficiency of photosynthesis and makes the plants more vulnerable to environmental fluctuations (Lawson and Blatt 2014; Tomeo and Rosenthal 2017; Silva *et al.* 2018; Wang *et al.* 2018). In this study, under high VPD, the OE lines demonstrated an increase in stomatal length, width, and individual area (Fig. 5-B–D), potentially augmenting the plants' capabilities for transpiration and gas exchange. This optimized stomatal morphology helps the plants utilize water more efficiently by regulating the transpiration rate to reduce water loss, while ensuring adequate CO_2 absorption to support photosynthesis. The stomatal density in the OE lines (Fig. 5-A) showed no significant difference compared to WT, indicating that although stomatal size increased, maintaining an appropriate stomatal density can balance the overall transpiration rate and CO_2 intake, thereby optimizing water and carbon dioxide use efficiency. Compared to WT and RNAi lines, the enhanced stomatal characteristics suggest that the *SlPIP1;7* overexpressing lines may have increased adaptability, enabling them to maintain a better physiological state under stress conditions such as high VPD. This improvement could enhance the plant's overall stress resistance by increasing the carbon assimilation rate while reducing water loss.

Research has shown that conditions of high VPD typically increase the rate of plant transpiration water loss, leading to stomatal closure to limit water loss and maintain water balance (Buckley 2016; Merilo *et al.* 2018; Jalakas *et al.* 2021). Although stomatal closure can prevent water loss through transpiration, it simultaneously restricts the absorption of CO_2 for photosynthesis, resulting in photosynthetic inhibition (Katul *et al.* 2009). In this study, overexpressing *SlPIP1;7* lines exhibited a significant increase in *A* (Fig. 4-A), indicating that plants could perform photosynthesis more effectively under high VPD conditions, converting more light energy into chemical energy. An observed significant increase in C_i (Fig. 4-C) suggests improved CO_2 absorption and utilization, corresponding with the increased rate of photosynthesis. The increase in g_{sw} indicates that the overexpressing lines could maintain higher stomatal openness under high VPD (Fig. 4-E), facilitating CO_2 absorption. It also implies plants' capability to optimize the balance between water transpiration and CO_2 acquisition. The significant improvement in $WUE_{instant}$ indicates that overexpressing lines could conduct more photosynthesis while consuming relatively less water (Fig. 4-F), showcasing an enhanced capacity for water use efficiency under stress conditions. The significant reductions in *E* and L_s (Fig. 4-B and D) further suggest that plants can maintain necessary stomatal openness while reducing water evaporation, which is advantageous in preventing excessive water loss and improving drought resistance. As mentioned, under high VPD, the stomatal closure and photosynthetic limitation in *SlPIP1;7* overexpressing plants are mitigated, thereby effectively maintaining CO_2 absorption from air to intercellular spaces.

Furthermore, additional analyses indicate that the enhanced stress resistance of *SlPIP1;7* is attributed not only to structural optimization but also to the precise regulation of physiological functions. Under high VPD conditions, a significant reduction in starch granules within the chloroplasts of tomato OE lines (Fig. 3-K–T) suggests that these plants improve carbon assimilation efficiency, facilitating the conversion of starch into other carbohydrates and preventing the excessive accumulation of photosynthetic products (Cuellar-Ortiz *et al.* 2008). The dynamic conversion between starch and soluble sugars may help maintain cell turgor pressure through osmoregulation (Flütsch *et al.* 2020), thereby alleviating the fluctuations in water potential induced by high VPD. These findings reveal that *SlPIP1;7* employs a dual regulatory model of "structural-metabolic" adaptation, transforming physiological structural adaptability into physiological advantages in stress resistance (Kaplan and Guy 2004; Nagao *et al.* 2005; Cuellar-Ortiz *et al.* 2008; Liu *et al.* 2019; Zhang H L *et al.* 2023).

4.3. Potential mechanisms of *SlPIP1;7* in acclimation and stress response to high VPD

ERFs are a class of transcription factors widely present in plants and belong to the AP2/ERF transcription factor superfamily. The expression of ERFs is induced when plants are subjected to stress. They function by specifically binding to *cis*-acting elements such as GCC-box or DRE/CRT in the promoters of downstream target genes. Recent studies have shown that ERF transcription factors not only regulate plant growth, development, and metabolic processes but also play a crucial role in enabling plants to cope with both abiotic stresses (such as drought, high salinity, low temperature) and biotic stresses (Licausi *et al.* 2013; Giuliano *et al*. 2014; Zhang *et al.* 2015).

In this study, we found that the transcription factor SlERF4 may regulate the expression of *SlPIP1;7* by binding to specific sites on its promoter. Results from Y1H assays (Fig. 9-B) and LUC assays (Fig. 9-C) demonstrated that SlERF4 exerts a significant transcriptional regulatory effect on *SlPIP1;7*. These findings are consistent with previous studies confirming that ERF transcription factors mediate stress-responsive gene regulation by recognizing GCC-box and DRE/CRT *cis*-elements (Zhang *et al.* 2016; Kumar *et al.* 2019). Additionally, we observed synchronized upregulation of SlERF4 and *SlPIP1;7* expression under high VPD conditions (Fig. 9-D). This suggests that SlERF4 may function as an upstream regulator, initially perceiving atmospheric drought stress and subsequently binding to and activating *SlPIP1;7* expression. These results provide mechanistic insights into the transcriptional regulation of *SlPIP1;7* under stress and highlight the role of ERF transcription factors in modulating stress-responsive genes (Trivedi *et al.* 2019; Zhu *et al.* 2020).

However, to fully elucidate SlERF4's function, future studies should employ approaches such as generating ERF mutants or spatiotemporal expression analyses. These experiments would clarify whether SlERF4 has direct physiological effects beyond *SlPIP1;7* regulation and uncover its broader roles in water stress adaptation. Such investigations are essential for defining SlERF4's core mechanisms in plant water homeostasis and stress responses.

5. Conclusion

SlPIP1;7 directly participates in the plant's stress response process to high VPD stress by influencing the accumulation of ROS and regulating stomatal morphological characteristics. The overexpression of *SlPIP1;7* not only enhances the efficiency of ROS clearance, protecting plant cells from oxidative damage but also enhances overall physiological regulation capacity by optimizing stomatal morphology for efficient utilization of water and carbon, enabling plants to adapt to adverse environments. Moreover, the transcription factor SlERF4, by binding to the *SlPIP1;7* promoter, regulates the expression of *SlPIP1;7*, further revealing the mechanism through which *SlPIP1;7* counters high VPD stress.

Acknowledgements

This work was supported by the Shaanxi Province Project on Key Core Technology Research in Agriculture, China (2023NYGG008) and the Construction of Qinchuangyuan "Scientist+Engineer" Team of Shaanxi Province, China (2023KXJ-024).

Declaration of competing interest

The authors declare that they have no conflict of interest.

Declaration of generative AI and AI-assisted technologies in the writing process

The authors declare that they did not use AI in the preparation and writing of this manuscript.

Appendices associated with this paper are available at https://doi.org/10.1016/j.jia.2026.04.020

References

Aroca R, Porcel R, Ruiz-Lozano J M. 2012. Regulation of root water uptake under abiotic stress conditions. *Journal of Experimental Botany*, **63**, 43–57.

Bai J, Wang X, Yao X, Chen X, Lu K, Hu Y, Wang Z, Mu Y, Zhang L, Dong H. 2021. Rice aquaporin *OsPIP2;2* is a water-transporting facilitator relevant to drought-tolerant responses. *Plant Direct*, **5**, e000338.

Bienert G P, Møller A L, Kristiansen K A, Schulz A, Møller I M, Schjoerring J K, Jahn T P. 2007. Specific aquaporins facilitate the diffusion of hydrogen peroxide across membranes. *Journal of Biological Chemistry*, **282**, 1183–1192.

Bienert M D, Bienert G P. 2017. Plant aquaporins and metalloids. In: Chaumont F, Tyerman S., eds., *Plant Aquaporins. Signaling and Communication in Plants.* Springer, Cham. pp. 297–332.

Buckley T N. 2016. Stomatal responses to humidity: Has the 'black box' finally been opened? *Plant*, *Cell & Environment*, **39**, 482–484.

Buckley T N. 2019. How do stomata respond to water status? New insights from rapid response gas exchange measurements. *Plant*, *Cell & Environment*, **42**, 1106–1122.

Carella A, Massenti R, Lo Bianco R. 2023. Testing effects of vapor pressure deficit on fruit growth: A comparative approach using peach, mango, olive, orange, and loquat. *Frontiers in Plant Science*, **14**, 1294195.

Chater C, Peng K, Movahedi M, Dunn J A, Walker H J, Liang Y K, McLachlan D H, Casson S, Isner J C, Wilson I, Neill S J, Hedrich R, Gray G E, Hetherington A M. 2015. Elevated CO_2-induced responses in stomata require ABA and ABA signaling. *Current Biology*, **25**, 2709–2716.

Chaumont F, Tyerman S D. 2014. Aquaporins: Highly regulated channels controlling plant water relations. *Plant Physiology*, **164**, 1600–1618.

Considine M J, Foyer C H. 2021. Stress effects on the reactive oxygen species-dependent regulation of plant growth and development. *Journal of Experimental Botany*, **72**, 5795–5806.

Cuellar-Ortiz S M, De La Paz Arrieta-Montiel M, Acosta-Gallegos J, Covarrubias A A. 2008. Relationship between carbohydrate partitioning and drought resistance in common bean. *Plant*, *Cell & Environment*, **31**, 1399–1409.

Ding J P, Jiao X C, Bai P, Hu Y X, Zhang J Y, Li J M. 2022. Effect of vapor pressure deficit on the photosynthesis, growth, and nutrient absorption of tomato seedlings. *Scientia Horticulturae*, **293**, 110736.

Ding L, Milhiet T, Parent B, Meziane A, Tardieu F, Chaumont F. 2022. The plasma membrane aquaporin *ZmPIP2;5* enhances the sensitivity of stomatal closure to water deficit. *Plant*, *Cell & Environment*, **45**, 1146–1156.

Du Y, Chen X K, Guo Y L, Zhang X J, Zhang H X, Li F F, Huang G Y, Meng Y L, Shan W X. 2021. *Phytophthora infestans* RXLR effector PITG20303 targets a potato MKK1 protein to suppress plant immunity. *New Phytologist*, **229**, 501–515.

Fakhet D, Morales F, Jauregui I, Erice G, Aparicio-Tejo P M, González-Murua C, Aroca R, Irigoyen J J, Aranjuelo I. 2021. Short-term exposure to high atmospheric vapor pressure deficit (VPD) severely impacts durum wheat carbon and nitrogen metabolism in the absence of edaphic water stress. *Plants*, **10**, 120.

Fan S, Han N, Wu H, Jia J, Guo J. 2021a. Plasma membrane intrinsic protein *SlPIP1;7* promotes root growth and enhances drought stress tolerance in transgenic tomato (*Solanum lycopersicum*) plants. *Plant Breeding*, **140**, 1102–1114.

Fan S, Wu H, Han N, Jia J, Guo J. 2021b. The role of *SlPIP1;7* in improving photosynthetic efficiency, root water uptake, and salt stress tolerance of tomato. *Horticultural Science and Technology*, **39**, 795–806.

Flütsch S, Wang Y Z, Takemiya A, Vialet-Chabrand S R M, Klejchová M, Nigro A, Hills A, Lawson T, Blatt M R, Santelia D. 2020. Guard cell starch degradation yields glucose for rapid stomatal opening in *Arabidopsis*. *The Plant Cell*, **32**, 2325–2344.

Franks P J, Farquhar G D. 2001. The effect of exogenous abscisic acid on stomatal development, stomatal mechanics, and leaf gas exchange in *Tradescantia virginiana*. *Plant Physiology*, **125**, 935–942.

Gautam A, Pandey A K. 2021. Aquaporins responses under challenging environmental conditions and abiotic stress tolerance in plants. *The Botanical Review*, **87**, 467–495.

Giuliano G, Liu M C, Bouzayen M, Pirrello J, Li Z G. 2014. The chimeric repressor version of an *Ethylene Response Factor* (*ERF*) family member, *Sl-ERF.B3*, shows contrasting effects on tomato fruit ripening. *New Phytologist*, **203**, 206–218.

Grossiord C, Buckley T N, Cernusak L A, Novick K A, Poulter B, Siegwolf R T W, Sperry J S, McDowell N G. 2020. Plant responses to rising vapor pressure deficit. *New Phytologist*, **226**, 1550–1566.

Groszmann M, Osborn H L, Evans J R. 2017. Carbon dioxide and water transport through plant aquaporins. *Plant*, *Cell & Environment*, **40**, 938–961.

Hoffert J D, Pisitkun T, Wang G, Shen R F, Knepper M A. 2006. Quantitative phosphoproteomics of vasopressin-sensitive renal cells: Regulation of aquaporin-2 phosphorylation at two sites. *Proceedings of the National Academy of Sciences of the United States of America*, **103**, 7159–7164.

Hooijmaijers C, Rhee J Y, Kwak K J, Chung G C, Horie T, Katsuhara M, Kang H. 2012. Hydrogen peroxide permeability of plasma membrane aquaporins of *Arabidopsis thaliana*. *Journal of Plant Research*, **125**, 147–153.

Hossain M A, Bhattacharjee S, Armin S M, Qian P W, Li H Y, Tran L S P. 2015. Hydrogen peroxide priming modulates abiotic oxidative stress tolerance: Insights from ROS detoxification and scavenging. *Frontiers in Plant Science*, **6**, 420.

Huang X S, Wang W, Zhang Q, Liu J H. 2013. A basic helix-loop-helix transcription factor, *PtrbHLH*, of *Poncirus trifoliata* confers cold tolerance and modulates peroxidase-mediated scavenging of hydrogen peroxide. *Plant Physiology*, **162**, 1178–1194.

Israel D, Khan S, Warren C R, Zwiazek J J, Robson T M. 2021. The contribution of PIP2-type aquaporins to photosynthetic response to increased vapour pressure deficit. *Journal of Experimental Botany*, **72**, 5066–5078.

Jalakas P, Takahashi Y, Waadt R, Schroeder J I, Merilo E. 2021.

Molecular mechanisms of stomatal closure in response to rising vapour pressure deficit. *New Phytologist*, **232**, 468–475.
Jing W, Li Y, Zhang S, Zhou X, Gao J, Ma N. 2023. Aquaporin, beyond a transporter. *Horticultural Plant Journal*, **9**, 29–34.
John G P, Scoffoni C, Buckley T N, Villar R, Poorter H, Sack L. 2017. The anatomical and compositional basis of leaf mass per area. *Ecology Letters*, **20**, 412–425.
Kaldenhoff R, Fischer M. 2006. Functional aquaporin diversity in plants. *Biochimica et Biophysica Acta*, **1758**, 1134–1141.
Kaplan F, Guy C L. 2004. β-amylase induction and the protective role of maltose during temperature shock. *Plant Physiology*, **135**, 1674–1684.
Katul G G, Palmroth S, Oren R. 2009. Leaf stomatal responses to vapour pressure deficit under current and CO_2 enriched atmosphere explained by the economics of gas exchange. *Plant*, *Cell & Environment*, **32**, 968–979.
Keenan T F, Hollinger D Y, Bohrer G, Dragoni D, Munger J W, Schmid H P, Richardson A D. 2013. Increase in forest water-use efficiency as atmospheric carbon dioxide concentrations rise. *Nature*, **499**, 324–327.
Koehler T, Wankmüller F J, Sadok W, Carminati A. 2023. Transpiration response to soil drying versus increasing vapor pressure deficit in crops: Physical and physiological mechanisms and key plant traits. *Journal of Experimental Botany*, **74**, 4789–4807.
Kozeko L Y. 2019. The role of HSP90 chaperones in stability and plasticity of ontogenesis of plants under normal and stressful conditions (*Arabidopsis thaliana*). *Cytology and Genetics*, **53**, 143–161.
Kumar M, Choi J, An G, Kim S R. 2019. Ectopic expression of *OsSta2* enhances salt stress tolerance in rice. *Frontiers in Plant Science*, **10**, 210.
Kurowska M M. 2021. Aquaporins in cereals-important players in maintaining cell homeostasis under abiotic stress. *Genes*, **12**, 477.
Lawson T, Blatt M R. 2014. Stomatal size, speed, and responsiveness impact on photosynthesis and water use efficiency. *Plant Physiology*, **164**, 1556–1570.
Li F, Xiao J F, Chen J Q, Ballantyne A, Jin K, Li B, Abraha M, John R. 2023. Global water use efficiency saturation due to increased vapor pressure deficit. *Science*, **381**, 672–677.
Li G, Santoni V, Maurel C. 2014. Plant aquaporins: Roles in plant physiology. *Biochimica et Biophysica Acta*, **1840**, 1574–1582.
Li G S, Han J L, Yi C, Luo H, Wang Y Z, Wang F P, Wang X Y, Chen L T, Zhang Y. 2024. Global characterization of OsPIP aquaporins reveals that the H_2O_2 transporter *OsPIP2;6* increases resistance to rice blast. *The Crop Journal*, **12**, 102–109.
Li S X, Liu J L, An Y R, Cao Y M, Liu Y S, Zhang J, Geng J C, Hu T M, Yang P Z. 2019. *MsPIP2;2*, a novel aquaporin gene from *Medicago sativa*, confers salt tolerance in transgenic *Arabidopsis*. *Environmental and Experimental Botany*, **165**, 39–52.
Li X T, Guo Y R, Ling Q P, Guo Z J, Lei Y W, Feng X M, Wu J Y, Zhang N N. 2024. Advances in the structure, function, and regulatory mechanism of plant plasma membrane intrinsic proteins. *Genes*, **16**, 10.
Licausi F, Ohme-Takagi M, Perata P. 2013. APETALA2/Ethylene Responsive Factor (AP2/ERF) transcription factors: Mediators of stress responses and developmental programs. *New Phytologist*, **199**, 639–649.
Liu J, Hu T, Fang L, Peng X, Liu F. 2019. CO_2 elevation modulates the response of leaf gas exchange to progressive soil drying in tomato plants. *Agricultural and Forest Meteorology*, **268**, 181–188.
Liu M, Wang C Y, Ji Z, Lu J Y, Zhang L, Li C L, Huang J G, Yang G D, Yan K, Zhang S Z, Zheng C C, Wu C G. 2023. Regulation of drought tolerance in *Arabidopsis* involves the PLATZ4-mediated transcriptional repression of plasma membrane aquaporin *PIP2;8*. *The Plant Journal*, **115**, 434–451.
Livak K J, Schmittgen T D. 2001. Analysis of relative gene expression data using realtime quantitative PCR and the $2^{-\Delta\Delta Ct}$ method. *Methods*, **25**, 402–408.
Majeed Y, Zhu X, Zhang N, Ul-Ain N, Raza A, Haider F U, Si H. 2023. Harnessing the role of mitogen-activated protein kinases against abiotic stresses in plants. *Frontiers in Plant Science*, **14**, 932923.
Mathias J M, Thomas R B. 2021. Global tree intrinsic water use efficiency is enhanced by increased atmospheric CO_2 and modulated by climate and plant functional types. *Proceedings of the National Academy of Sciences of the United States of America*, **118**, e2014286118.
Matsumoto T, Lian H L, Su W A, Tanaka D, Liu C W, Iwasaki I, Kitagawa Y. 2009. Role of the aquaporin PIP1 subfamily in the chilling tolerance of rice. *Plant and Cell Physiology*, **50**, 216–229.
Maurel C, Boursiac Y, Luu D T, Santoni V, Shahzad Z, Verdoucq L. 2015. Aquaporins in plants. *Physiological Reviews*, **95**, 1321–1358.
Maurel C, Plassard C. 2011. Aquaporins: For more than water at the plant-fungus interface? *New Phytologist*, **190**, 815–817.
Medina S, Vicente R, Amador A, Araus J L. 2016. Interactive effects of elevated [CO_2] and water stress on physiological traits and gene expression during vegetative growth in four durum wheat genotypes. *Frontiers in Plant Science*, **22**, 1738.
Merilo E, Yarmolinsky D, Jalakas P, Parik H, Tulva I, Rasulov B, Kilk K, Kollist H. 2018. Stomatal VPD response: There is more to the story than ABA. *Plant Physiology*, **176**, 851–864.
Nagao M, Minami A, Arakawa K, Fujikawa S, Takezawa D. 2005. Rapid degradation of starch in chloroplasts and concomitant accumulation of soluble sugars associated with ABA-induced freezing tolerance in the moss *Physcomitrella patens*. *Plant Physiology*, **162**, 169–180.
Olesen E T, Fenton R A. 2021. Aquaporin 2 regulation: Implications for water balance and polycystic kidney diseases. *Nature Reviews Nephrology*, **17**, 765–781.
Pérez-Bueno M L, Pineda M, Díaz-Casado E, Barón M. 2015. Spatial and temporal dynamics of primary and secondary metabolism in *Phaseolus vulgaris* challenged by *Pseudomonas syringae*. *Physiologia Plantarum*, **153**, 161–174.
Ravi B, Foyer C H, Pandey G K. 2023. The integration of reactive oxygen species (ROS) and calcium signalling in abiotic stress responses. *Plant*, *Cell & Environment*, **46**, 1985–2006.
Rodriguez-Dominguez C M, Buckley T N, Egea G, de Cires A, Hernandez-Santana V, Martorell S, Diaz-Espejo A. 2016. Most stomatal closure in woody species under moderate drought can be explained by stomatal responses to leaf turgor. *Plant*, *Cell & Environment*, **39**, 2014–2026.
Silva G S, Gavassi M A, Nogueira M A, Habermann G. 2018. Aluminum prevents stomatal conductance from responding to vapor pressure deficit in *Citrus limonia*. *Environmental and Experimental Botany*, **155**, 662–671.
Smirnoff N, Arnaud D. 2019. Hydrogen peroxide metabolism and functions in plants. *New Phytologist*, **221**, 1197–1214.
Sun X, Deng Y, Liang L, Jia X, Xiao Z, Su J. 2017. Overexpression of a *PIP1* gene from *Salicornia bigelovii* in tobacco plants improves their drought tolerance. *American Society for Horticultural Science Journal*, **142**, 235–245.
Tamang B G, Zhang Y Q, Zambrano M A, Ainsworth E A. 2023. Anatomical determinants of gas exchange and hydraulics vary with leaf shape in soybean. *Annals of Botany*, **131**, 909–920.
Tchakal-Mesbahi A, He J, Zhu S, Huang M, Fukushima K, Bouley R, Brown D, Lu H A. 2024. Focal Adhesion Kinase (FAK) inhibition induces membrane accumulation of aquaporin2 (AQP2) through endocytosis inhibition and actin depolymerization in renal epithelial cells. *bioRxiv*, doi: https://doi.org/10.1101/2024.10.08.617300
Tomeo N J, Rosenthal D M. 2017. Variable mesophyll conductance among soybean cultivars sets a tradeoff between photosynthesis and water-use-efficiency. *Plant Physiology*, **174**, 241–257.
Törnroth-Horsefield S, Wang Y, Hedfalk K, Johanson U, Karlsson M, Tajkhorshid E, Neutze R, Kjellbom P. 2006. Structural mechanism of plant aquaporin gating. *Nature*, **439**, 688–694.
Trivedi P, Nguyen N, Hykkerud A L, Häggman H, Martinussen I, Jaakola L, Karppinen K. 2019. Red and blue light signaling regulate fruit anthocyanin biosynthesis in relation to the circadian rhythm in bilberry. *Frontiers in Plant Science*, **10**, 1133.
Vadez V, Kholova J, Medina S, Kakkera A, Anderberg H. 2014. Transpiration efficiency: New insights into an old story. *Journal of Experimental Botany*, **6**, 6141–6153.
Veal E A, Day A M, Morgan B A. 2007. Hydrogen peroxide sensing and signaling. *Molecular Cell*, **26**, 1–14.
Wang S, Zhang Y, Ju W, Chen J M, Ciais P, Cescatti A, Sardans J, Janssens I A, Wu M, Berry J A, Campbell E, Fernández-Martínez M, Alkama R, Sitch S, Friedlingstein P, Smith W K, Yuan W, He W, Lombardozzi D, Kautz M, *et al.* 2020. Recent global decline of CO_2 fertilization effects on vegetation photosynthesis. *Science*, **370**, 1295–1300.

Wang X X, Du T T, Huang J L, Peng S B, Xiong D L. 2018. Leaf hydraulic vulnerability triggers the decline in stomatal and mesophyll conductance during drought in rice. *Journal of Experimental Botany*, **69**, 4033–4045.

Xu Z, Zhou G. 2008. Responses of leaf stomatal density to water status and its relationship with photosynthesis in a grass. *Journal of Experimental Botany*, **59**, 3317–3325.

Yamanaka R, Yano T, Hikawa-Endo M, Yoshikoshi H, Kawashima H, Tojo M, Wada T. 2024. Effects of humidification based on vapor pressure deficit (VPD) on plant growth, fruit yield, and fruit quality traits in June-bearing strawberry. *The Horticulture Journal*, **93**, 377–388.

Yong J, Wong S, Farquhar G. 1997. Stomatal responses to changes in vapour pressure difference between leaf and air. *Plant*, *Cell & Environment*, **20**, 1213–1216.

Yu F F, Liu C X, Zhang H L, Xie Q. 2023. AG protein γ subunit regulates crop alkaline sensitivity by modulating H_2O_2 transporter PIP2s. *Journal of Molecular Cell Biology*, **15**, mjad020.

Yu X M, Niu L Q, Zhang Y H, Xu Z J, Zhang J W, Zhang S H, Li J M. 2024. Vapour pressure deficit affects crop water productivity, yield, and quality in tomatoes. *Agricultural Water Management*, **299**, 108879.

Yu X M, Zhang Y H, Zhao X F, Li J M. 2023. Systemic effects of the vapor pressure deficit on the physiology and productivity of protected vegetables. *Vegetable Research*, **3**, 1.

Yu X M, Zhao M F, Wang X Y, Jiao X C, Song X M, Li J M. 2022. Reducing vapor pressure deficit improves calcium absorption by optimizing plant structure, stomatal morphology, and aquaporins in tomatoes. *Environmental and Experimental Botany*, **195**, 104786.

Yuan W, Zheng Y, Piao S, Ciais P, Lombardozzi D, Wang Y, Ryu Y, Chen G, Dong W, Hu Z, Jain A K, Jiang C, Kato E, Li S, Lienert S, Liu S, Nabel J E M S, Qin Z, Quine T, Sitch S, *et al.* 2019. Increased atmospheric vapor pressure deficit reduces global vegetation growth. *Science Advances*, **5**, eaax1396.

Zhang D L, Du Q J, Zhang Z, Jiao X C, Song X M, Li J M. 2017. Vapour pressure deficit control in relation to water transport and water productivity in greenhouse tomato production during summer. *Scientific Reports*, **7**, 43461.

Zhang D L, Jiao X C, Du Q J, Song X M, Li J M. 2018. Reducing the excessive evaporative demand improved photosynthesis capacity at low costs of irrigation via regulating water driving force and moderating plant water stress of two tomato cultivars. *Agricultural Water Management*, **199**, 22–33.

Zhang D L, Yang H H, Chen X L, Li Y , Li Y Z, Liu H Y, Wu X L, Wei M. 2024. VPD modifies CO_2 fertilization effect on tomato plants via abscisic acid and jasmonic acid signaling pathways. *Horticultural Plant Journal*, **10**, 1165–1176.

Zhang D L, Zhang Z, Li J M, Chang Y B, Du Q J, Pan T H. 2015. Regulation of vapor pressure deficit by greenhouse micro-fog systems improved growth and productivity of tomato via enhancing photosynthesis during summer season. *PLoS ONE*, **10**, e0133919.

Zhang H L, Yu F F, Xie P, Sun S Y, Qiao X H, Tang S Y, Chen C X, Yang S, Mei C, Yang D K, Wu Y R, Xia R, Li X, Lu J, Liu Y X, Xie X W, Ma D M, Xu X, Liang Z W, Feng Z H, *et al.* 2023. A Gγ protein regulates alkaline sensitivity in crops. *Science*, **379**, eade8416.

Zhang L N, Zhang L C, Xia C, Zhao G Y, Jia J Z, Kong X Y. 2016. The novel wheat transcription factor TaNAC47 enhances multiple abiotic stress tolerances in transgenic plants. *Frontiers in Plant Science*, **6**, 1174.

Zhang M, Shi H T, Li N N, Wei N N, Tian Y, Peng J F, Chen X C, Zhang L Y, Zhang M X, Dong H S. 2022. Aquaporin *OsPIP2;2* links the H_2O_2 signal and a membrane-anchored transcription factor to promote plant defense. *Plant Physiology*, **188**, 2325–2341.

Zhang X, Liu X X, Wu L, Yu G H, Wang X, Ma H X. 2015. The *SsDREB* transcription factor from the succulent halophyte *Suaeda salsa* enhances abiotic stress tolerance in transgenic tobacco. *International Journal of Genomics*, **2015**, 875497.

Zhang Y H, Zhao X F, Li B, Liu C, Yu X M, Zhang Z D, Zhang S H, Li J M. 2024. Plasma membrane intrinsic proteins *SlPIP2;5* gene regulates tolerance to high VPD in tomato. *Environmental and Experimental Botany*, **222**, 105771.

Zhang Y, Zhu J, Khan M, Wang Y, Xiao W, Fang T, Qu J, Xiao P, Li C, Liu J H. 2023. Transcription factors ABF4 and ABR1 synergistically regulate amylase-mediated starch catabolism in drought tolerance. *Plant Physiology*, **191**, 591–609.

Zhang Z D, Dang J, Yuan L Q, Zhang Y H, Zhou F, Liu T, Li T L, Hu X H. 2023. Exogenous 5-Aminolevulinic acid improved low-temperature tolerance tomato seedling by regulating starch content and phenylalanine metabolism. *Plant Physiology and Biochemistry*, **210**, 108083.

Zhang Z D, Yuan L Q, Dang J, Zhang Y H, Wen Y S, Du Y, Liang Y F, Wang Y, Liu T, Li T L, Hu X H. 2024. 5-Aminolevulinic acid improves cold resistance through regulation of *SlMYB4*/*SlMYB88-SlGSTU43* module to scavenge reactive oxygen species in tomato. *Horticultural Research*, **11**, uhae026.

Zhang Z D, Yuan L Q, Ma Y B, Kang Z, Zhou F, Gao Y, Yang S C, Li T L, Hu X H. 2022. Exogenous 5-aminolevulinic acid alleviates low-temperature damage by modulating the xanthophyll cycle and nutrient uptake in tomato seedlings. *Plant Physiology and Biochemistry*, **189**, 83–93.

Zhang Z, Cao B, Li N, Chen Z, Xu K. 2019. Comparative transcriptome analysis of the regulation of ABA signaling genes in different rootstock grafted tomato seedlings under drought stress. *Environmental and Experimental Botany*, **166**, 103814.

Zhou L, Zhou J, Xiong Y H, Liu C X, Wang J G, Wang G Q, Cai Y L. 2019. Overexpression of a maize plasma membrane intrinsic protein ZmPIP1;1 confers drought and salt tolerance in Arabidopsis. *PLoS ONE*, **13**, e0198639.

Zhou W J, Leul M. 1998. Uniconazole-induced alleviation of freezing injury in relation to changes in hormonal balance, enzyme activities and lipid peroxidation in winter rape. *Plant Growth Regulation*, **26**, 41–47.

Zhu H, Bao Y Z, Peng H, Li X L, Pan W Y, Yang Y F, Kuang Z F, Ji P Y, Liu J D, Shen D Y, Ai G, Dou D L. 2025. Phosphorylation of PIP2;7 by CPK28 or *Phytophthora* kinase effectors dampens pattern-triggered immunity in *Arabidopsis*. *Plant Communications*, **6**, 101135.

Zhu J K. 2020. Abiotic stress signaling and responses in plants. *Cell*, **181**, 368–394.

Executive Editor-in-Chief Sanwen Huang
Managing Editor Lingyun Weng